Experimental and Process Simulation Study on the Production of Magnesium Hydroxide and Magnesium Oxide from Seawater Reverse Osmosis Brine

Abstract

Brine disposal poses a major environmental challenge in the desalination sector due to its high concentrations of salts and chemical additives. Among these, magnesium represents a valuable resource that can be recovered via precipitation, reducing costs and mitigating environmental impact. This study investigates magnesium recovery from brine through the precipitation of $Mg^{+٢}$ as $Mg(OH)_2$ and its subsequent conversion to MgO. A systematic experimental design using Response Surface Methodology (RSM) with a central composite design was applied to evaluate the effects of NaOH concentration (٥–١٠ g/L) and precipitation temperature (٦٠–٩٠ °C) on magnesium precipitation efficiency. Analysis of variance (ANOVA) confirmed that NaOH concentration has a statistically significant effect on magnesium precipitation, while temperature and interaction terms were negligible. Aspen Plus simulations quantified the effects of feed flow rate, precipitation temperature, and NaOH concentration on NaOH consumption, product yields, energy demand, water generation, and economic analysis. Increasing feed flow rate from ٥٠,٠٠٠ m^3/day to ١٠٠,٠٠٠ m^3/day doubled $Mg(OH)_2$ production (١٣١–٢٦٣ t/day), MgO production (٩١–١٨٢ t/day), and water generation (١٥٠–٣٠٠ m^3/day), while NaOH consumption rose from ٣٧٥ t/day to ٧٥٠ t/day, and energy demand increased from ١٢,٠٠٠ kW to ٤٤,٠٠٠ kW. Raising the precipitation temperature from ٦٠ °C to ٩٠ °C keeps $Mg(OH)_2$ and MgO production almost stable but increases energy demand by approximately ٢,٣ times. Increasing NaOH concentration from ٥ g/L to ١٠ g/L doubled $Mg(OH)_2$ and MgO production, increased revenue by 117%, and slightly decreased net energy consumption (~3.7%). Economic analysis showed that maximum feed flow rate, high NaOH concentration, and low precipitation temperature (60°C) yielded the highest net annual profit (~133 million USD).

Keywords: Magnesium recovery, Brine water, MgO production, Process simulation, Aspen Plus

1. Introduction

Tackling water scarcity is a major concern for many countries around the world [1-3]. In response, increasing attention has turned to alternative water sources, especially seawater, to meet the growing demand for drinking and agricultural use [4]. Among these solutions, seawater desalination has gained prominence as a viable option with significant potential for large-scale development and investment. Reverse osmosis (RO) systems are extensively used for seawater desalination and industrial wastewater treatment. A major byproduct of these systems is brine, which is a concentrated saline waste stream containing high levels of dissolved salts, including significant concentrations of magnesium ions (Mg^{+2}). Instead of being discarded, brine can be utilized as a valuable resource for recovering useful compounds, particularly magnesium. In addition to brine, seawater and geothermal water are also considered abundant and practically limitless sources of magnesium [5].

On an industrial scale, magnesium is typically recovered through a precipitation process. This involves reacting the magnesium ions in solution with dolime, which is a mixture of calcium oxide and magnesium oxide produced by the thermal decomposition of dolomite ($CaMg(CO_3)_2$) or magnesite ($MgCO_3$). This reaction leads to the formation of solid magnesium hydroxide ($Mg(OH)_2$), which can be separated from the liquid phase [٦]. In some processes, sodium hydroxide (NaOH) is added to enhance the precipitation of magnesium hydroxide, especially when higher purity or more complete recovery is required. The addition of NaOH increases the pH of the solution, shifting the equilibrium toward the formation of $Mg(OH)_2$ and improving the efficiency of the separation process [7]. The collected magnesium hydroxide is then subjected to a high-temperature calcination process, where it decomposes into high-purity magnesium oxide (MgO) [8]. This final product is widely used in the production of refractory materials, environmental technologies, and various chemical applications [9]. Overall, this approach not only adds economic value to waste streams but also supports sustainable and efficient recovery of valuable materials from saline water sources [10]. Several researchers have investigated the production of magnesium hydroxide, and some studies have also examined its thermal decomposition to produce magnesium oxide.

Lehmann et al. [١١] introduced a magnetite-based recovery system for extracting $Mg^{+٢}$ from high-salinity first-stage seawater reverse osmosis brine. Magnesium was precipitated as $Mg(OH)_2$ onto Fe_3O_4 particles, magnetically separated, and later redissolved using acid to regenerate a high-purity magnesium solution (>97%). Sorour et al. [12] focused their research on modifying industrial processes to improve the recovery of magnesium-containing by-products. They conducted experiments using various precipitation reagents and process configurations. Specifically, they examined the partial softening of seawater and reverse osmosis brines by applying Na_2CO_3 and Na_3PO_4 to precipitate calcium and magnesium. Casas et al. [١٣] investigated the use of Na_2CO_3 and NaOH as alkaline reagents to recover $Mg^{+٢}$ and Ca^{2+} from mining and seawater desalination brines. Their results indicated that adding Na_2CO_3 at pH levels above ١٠ enabled Ca recovery rates exceeding ٩٤–٩٦٪, while NaOH dosing at pH levels above ١١ achieved Mg recovery rates greater than ٩٧–٩٩٪. Ahmed et al. [١٤] evaluated mineral recovery from seawater reverse osmosis brine using precipitation and identified sodium hydroxide as the most effective base. Turek and Gnot [15] conducted a series of

experiments in which a precipitating agent was added to a magnesium ion solution without stirring, across various temperatures. Their findings revealed that lower temperatures and higher concentrations of the precipitant led to a quicker precipitation and sedimentation process, which in turn enhanced the filtration rate. Martel et al. [١٦] designed an efficient process capable of reusing approximately ٨,٤٠٠ m^3 of brine per day. In this method, calcium present as $CaCl_2$ and sulfates present as Na_2SO_4 were effectively removed through precipitation by adding sodium carbonate (Na_2CO_3) and barium chloride ($BaCl_2$) solutions. Mohammad et al. [٦] successfully recovered $Mg(OH)_2$ from desalination reject brines by using NH_4OH as the precipitating agent. In their process, magnesium carbonate ($MgCO_3$), a primary component of the brine, reacted with NH_4OH to form magnesium hydroxide. Dong et al. [٧] studied the recovery of reactive magnesium oxide (MgO) from reject brine, a waste product of desalination. They precipitated $Mg(OH)_2$ by reacting $Mg^{+٢}$ in the brine with NaOH, optimizing the NaOH-to-$Mg^{+٢}$ ratio to maximize yield. The $Mg(OH)_2$ was then calcined at temperatures between ٥٠٠ and ٧٠٠ °C for ٢ to ١٢ hours to produce reactive MgO. Ashraf et al. [١٧] studied the production of reactive MgO from reject brine using ammonia and sodium hydroxide as precipitants. They found that MgO from ammonia-produced $Mg(OH)_2$ had higher surface area and reactivity, especially when calcined at ٥٠٠ °C for ٢ hours, compared to NaOH-based MgO. Dong et al. [١٨] demonstrated the successful synthesis of high-purity, reactive MgO from reject brine using NH_4OH. Optimizing the NH_4OH to $Mg^{+٢}$ ratio at ٦ yielded Mg $(OH)_2$ with ٩٣,٥٪ purity, which was calcined at ٥٠٠ °C for ٢ hours to produce MgO with a specific surface area of ٧٨,٨ m^2/g. Xiao et al. [١٩] demonstrated a sustainable method for recovering MgO from reject brine using waste concrete sludge as an alkali source. Alkaline water (pH 12.2) extracted from the sludge enabled ٩٤٪ $Mg^{+٢}$ recovery as brucite, which was then calcined at ٥٠٠ °C to produce high-purity MgO (>٨٠٪) with a surface area >٧٥ m^2/g. This process showed significantly lower energy use and carbon emissions than conventional methods. Karmil et al. [٢٥] investigated the recovery of reactive CaO and MgO from RO reject brine rich in Ca^{2+} and Mg^{+2}. Using selective precipitation, they achieved 97.5% calcium oxalate recovery with oxalic acid and ٩٧٪ brucite recovery with NaOH. The precipitates were calcined to produce quicklime and magnesia, with BET surface areas of ١٠,٤ m^2/g and ٥٨,٣ m^2/g, respectively. Modeling and cost analysis confirmed the process as efficient and sustainable, highlighting RO brine as a valuable source for producing high-reactivity alkaline earth oxides.

Previous studies on magnesium recovery from brine have mainly focused on laboratory scale investigations, particularly the precipitation of magnesium hydroxide and its subsequent thermal decomposition into magnesium oxide. However, these processes have generally been studied separately, with limited attention given to their integration within an industrial scale framework. To achieve economic feasibility and industrial applicability, it is necessary to evaluate the complete recovery pathway, including magnesium ion removal from brine streams such as reverse osmosis effluents, $Mg(OH)_2$ precipitation, and its conversion into MgO.

The novelty of the present study lies in the integration of experimental investigation, Aspen Plus V12.1 process simulation, and industrial scale economic analysis into a unified framework for magnesium recovery from brine water. Experimental data obtained at laboratory scale were incorporated to improve the reliability and accuracy of the simulation model. In addition, a

comprehensive economic assessment was conducted to evaluate the feasibility and cost effectiveness of large-scale magnesium recovery and MgO production.

2. Materials and Methods

2.1. Experimental

In this study, magnesium precipitation from seawater reverse osmosis (SWRO) brine using sodium hydroxide (NaOH) was experimentally investigated, with particular focus on the effects of temperature and NaOH concentration, as these factors significantly influence magnesium recovery. All chemicals and reagents were obtained from Sigma-Aldrich (India) and Merck (Germany) and were used without further purification. Quantitative and qualitative analyses were performed under standard laboratory conditions using ICP-OES (iCAP 6000, Thermo Scientific, USA), a conductivity meter (ORION STAR A222), a spectrophotometer (LANGE DR ٢٨٠٠), and a pH meter (ORION STAR A٢٢١).

Brine samples were collected from the Shuwaikh SWRO desalination plant in Kuwait. The total dissolved solids (TDS) of the rejected brine were approximately 78,000 ppm. The average composition of feedwater and SWRO brine is presented in Table ١.

Precipitation experiments were carried out using a laboratory-scale assembly, as shown in Fig. 1. One liter of SWRO brine was placed in a glass beaker equipped with a magnetic stirrer. Sodium hydroxide was prepared as an aqueous solution at different concentrations and was added gradually in a controlled manner (dropwise addition) to the brine under continuous stirring to ensure uniform mixing and to avoid local supersaturation. The NaOH concentration range investigated was systematically varied to evaluate its effect on magnesium precipitation. The solution was continuously stirred for 15 minutes while the pH was monitored until stabilization. After reaching the desired pH, the mixture was transferred to a closed vessel and placed in an oven at a controlled temperature (٦٠–٩٠°C) for ١ hour to promote precipitation.

Following thermal treatment, the suspension was cooled to room temperature. The precipitated magnesium hydroxide was then separated from the liquid phase using vacuum filtration. The collected solid was thoroughly washed with deionized water to remove residual ions and impurities, and subsequently dried in an oven prior to further analysis. The filtrate was retained for residual magnesium analysis to evaluate recovery efficiency. The dried precipitate was then left for 6 hours to allow further crystallization and growth of the solid phase where applicable.

All experiments were conducted in triplicate, and the mean values were reported to ensure reproducibility. The effects of NaOH concentration and temperature on magnesium precipitation were systematically evaluated to determine the optimal conditions for maximum recovery. The final precipitate at four different pH values at 90°C is illustrated in Fig. 2.

Table 1: Average composition of effluent from the RO plant in of Shuwaikh brine

Component	Composition (mg/L)
Alkalinity	179
Boron	11
Calcium	1040
Lithium	2
Magnesium	2703
Potassium	1142
Sodium	27,802
Sulfate	7497

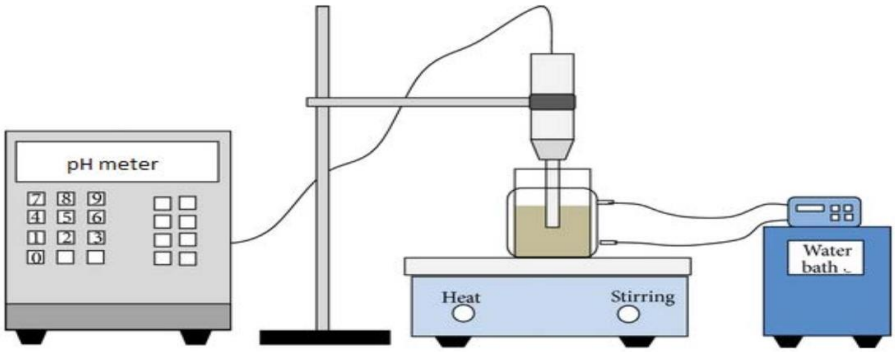

Fig. 1. Experimental setup for magnesium precipitation.

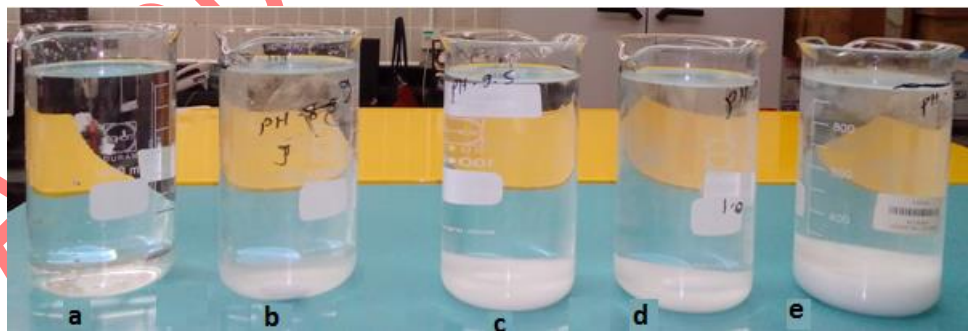

Fig. 2: Minerals precipitated at 90°C under different pH conditions: (a) pH 8.0, (b) pH 8.5, (c) pH 9.0, (d) pH 9.5, and (e) pH 10.0.

2.2. Design of Experiment (DOE)

To examine the influence of temperature and NaOH concentration on magnesium precipitation and pH, a systematic experimental design was employed. The design of experiments (DOE) approach allowed efficient planning of the tests and provided a structured framework for

statistical analysis. The response surface methodology (RSM) with a central composite (CC) design was applied to model and optimize the process. Analysis of variance (ANOVA) was used to evaluate the statistical significance of the factors and their interactions, and a mathematical model was developed to describe the relationship between the independent variables and the magnesium precipitation response. The response variable for this study was the magnesium precipitation efficiency, defined as:

$$\text{Magnesium Precipitation (\%)} = \frac{Mg^{+٢}_{initial} - Mg^{+٢}_{precipitated}}{Mg^{+٢}_{initial}} \times ١٠٠ \quad (١)$$

where Mg^{+2} represents the magnesium concentration in the brine, measured in mg/L. The factors investigated were temperature and NaOH concentration. Temperature levels were set at 60°C, 75°C, and 90°C, while NaOH concentration levels were selected as 5 g/L, 7.5 g/L, and 10 g/L. Table 2 presents the recommended experimental runs obtained from the RSM design, including four repetitions at the center point. Based on this design, magnesium precipitation experiments were conducted, and the corresponding results are summarized in Table 2.

Table 2: The factors and their corresponding results

Temperature (°C)	NaOH concentration (g/l)	Magnesium Precipitation (%)
75	7.5	75
75	10	95
90	10	95
90	5	44
75	7.5	76
75	7.5	74
75	7.5	75
75	5	47
60	5	51
60	10	95
60	7.5	75
90	7.5	73

2.3. Process simulation

This study investigates the production of magnesium hydroxide and magnesium oxide using Aspen Plus software (version 12.1). The analysis focuses on mass and energy balances, along with the economic performance of the process. The composition presented in Table 1 represents the key dissolved components in the brine stream discharged from a typical RO plant outlet. The main objective is to extract Mg^{+2} ions from brine using sodium hydroxide. The effects of brine mass flow rate and precipitation temperature were analyzed to identify the most cost-effective approach. The ENRTL-RK thermodynamic model is used to simulate water containing dissolved ions, as it is widely recommended for electrolyte systems [30-33] .

2.4. The precipitation of Mg^{+2}

A chemical precipitation method is used to recover magnesium from brine. Alkaline solution (sodium hydroxide) is added to the brine. This reaction leads to the formation of insoluble magnesium hydroxide, which precipitates out. The precipitate is then separated from the liquid via filtration. The reaction of this process is as follows:

$$Mg^{+٢} + ٢OH^{-} \rightarrow Mg(OH)_{٢} \quad (2)$$

To determine the percentage of Mg^{+2} precipitated in the reactor, the experimental data presented in the previous section were used.

2.5. Calcination to form MgO

Magnesium hydroxide is calcined, which means it is heated in a furnace at high temperatures to undergo thermal decomposition. During this process, chemically bound water molecules are removed, resulting in the formation of magnesium oxide (MgO) as a fine white powder. The chemical reaction for this process is as follows:

$$Mg(OH)_{٢} \rightarrow MgO + H_{٢}O \quad (3)$$

According to the study by Pan et al. [٣٤], the thermal decomposition of $Mg(OH)_2$ into MgO and water vapor reaches approximately 98% conversion at around 500 °C. This temperature has been widely reported in the literature as an effective operating condition for achieving a balance between high conversion efficiency and reasonable energy demand in $Mg(OH)_2$ calcination systems. In addition to Pan et al. [٣٤], several studies have reported that $Mg(OH)_2$ decomposition typically occurs in the range of ٣٥٠–٥٥٠ °C depending on particle size, heating rate, and impurities, with negligible improvement in conversion above 500 °C under atmospheric conditions.

Based on this well-established thermal behavior, 500 °C was selected as the calcination setpoint in the present study. This choice is justified not only by literature evidence but also by preliminary sensitivity checks performed within the simulation framework, which showed that increasing the temperature beyond 500 °C leads to only marginal improvement in MgO yield while significantly increasing the energy consumption of the calcination unit. Therefore, operating at higher temperatures does not provide a meaningful gain in conversion efficiency and is not economically favorable for large-scale application.

Furthermore, the selected temperature is consistent with industrial MgO production practice, where calcination processes are typically optimized to maximize energy efficiency rather than solely targeting maximum theoretical conversion. This ensures that the adopted operating condition is applicable to real industrial systems, where energy integration and cost minimization are critical factors. As a result, 500 °C represents an optimal compromise between conversion efficiency, energy demand, and process feasibility in the proposed magnesium recovery route.

2.6. Process flowsheet

Fig.3 illustrates the process design for recovering Mg^{+2} to produce MgO from brine water. In this design, the brine is first heated to the desired temperature (٦٠–٩٠ °C) based on our experimental study. At the beginning, the brine water from the RO plant is heated to the desired reaction temperature using a heat exchanger, which recovers energy from the effluent of Reactor ١ where $Mg(OH)_2$ is precipitated. Sodium hydroxide (NaOH) is added to Reactor ١ (R1), to magnesium precipitation. The experimental data obtained in our previous section were used to define this section. The outlet stream from Reactor 1 contains a mixture of liquid and solid magnesium hydroxide, along with small amounts of other co-precipitated compounds. This stream is passed through a filtration unit to separate the solids from the liquid. The filtrate can be directed to additional recovery processes, such as membrane distillation, reverse osmosis, or evaporation, to extract any remaining valuable compounds. Part of the recovered heat is also used for preheating the brine water.

The solid product requires washing to remove impurities. The resulting $Mg(OH)_2$ is obtained as a filter cake containing, on average, about 45% water [7, 25, 35], which must be removed. To achieve this, the solid is dried by heating to 105 °C to evaporate the water. The moisture content of the solid stream is controlled according to design specifications and Fortran-based calculations. After drying, the solid is introduced into Reactor 2, where it is further heated to ٥٠٠ °C, following the studies of Du et al. [٣٥], Dong et al. [٧], and Karmin et al. [٢٥], for the calcination of $Mg(OH)_2$ to MgO. The water vapor produced during calcination is recovered and used to preheat the reactor feed. This vapor is also combined with the dryer off-gas stream to enhance the energy efficiency of the drying process. The total water vapor is condensed to produce pure water. Table 3 illustrates the equipment used in the process simulation.

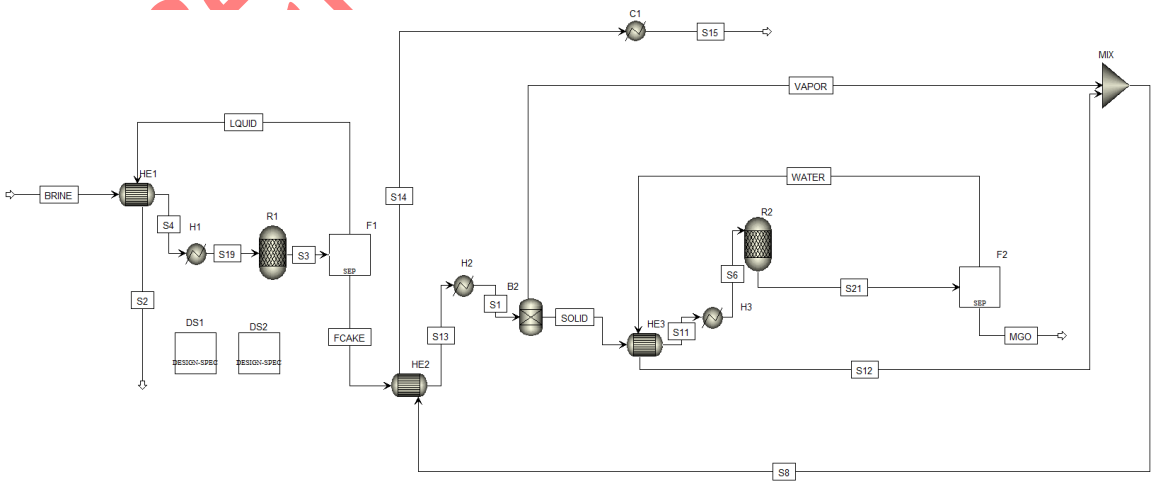

Fig. 3: Process flowsheet for the production of MgO from brine water

Table 3: List of equipment and Aspen Plus design specifications used in the process flowsheet

Legend	Equipment
HE1	Shell-and-tube heat exchanger
H1	Heater
R1	Precipitation reactor
F1	Solid–liquid separator
HE2	Shell-and-tube heat exchanger
H2	heater
B2	Solid–vapor separator
HE3	Shell-and-tube heat exchanger
H3	Heater
R2	Calcination reactor
C1	Cooler
DS1	Design Spec – control water cake flow
DS2	Design Spec – control heat exchanger area

3. Results and discussions

3.1. Experimental results

In this section, the experimental results are investigated. According to Table 2, the precipitation of magnesium is calculated as a function of temperature and NaOH concentration. The ANOVA table for the experimental results is illustrated in Table 4**.** According to the results, the quartic model, the NaOH concentration and A^2 are statistically significant. The high F-values indicate that factors have a strong influence on the response variable, while the low p-values (less than 0.05) confirm their significance at the 95% confidence level. This means that the quartic model correctly shows the nonlinear relationship between the factors. Changes in NaOH concentration, temperature, and their interaction, as well as the square term of A^2, have a clear effect on the percentage of magnesium precipitated. However, the squared term of B^2 is not important because its F-value is low and its p-value is higher than 0.05. This shows that this term has little influence on the response variable. Moreover, the lack of fit is not significant, as its F-value is low and the p-value is greater than 0.05. This indicates that the model fits the experimental data well, and there is no evidence of a systematic deviation between the predicted and observed values.

Table 4: ANOVA of the experiential results

Source	F-value	p-value
Model	143.9	<0.0001
A: NaOH (g/l)	713.2	<0.0001
B: Temperature (°C)	20.9	0.0038
AB	18.9	0.0048
A^2	47.0	0.0005
B^2	0.5	0.4749
Lack of Fit	1.0	0.5205

According to the table results, the model for predicting the percentage of magnesium precipitation is as follows:

$$R = -٢.٧٠٨ + ١٤.١٣٣A - ٠.٢٠٠B + ٠.٠٤٦AB - ٠.٥٤٠A^{٢} - ٠.٠٠١B^{٢} \quad (4)$$

Where R is the percentage of magnesium precipitated, A is the NaOH concentration (g/L), and B is the temperature (°C).

The coefficients of B, AB, and $B^{٢}$ are significantly lower than that of A. Therefore, the effect of A is considerably higher than the effects of the other terms.

Fig. 4 shows the comparison between the experimental magnesium precipitation data and the predictions of the developed model. The close alignment between the two demonstrates that the model accurately captures the behavior of the system, which is further supported by a high R^2 value of 0.99, indicating excellent predictive capability.

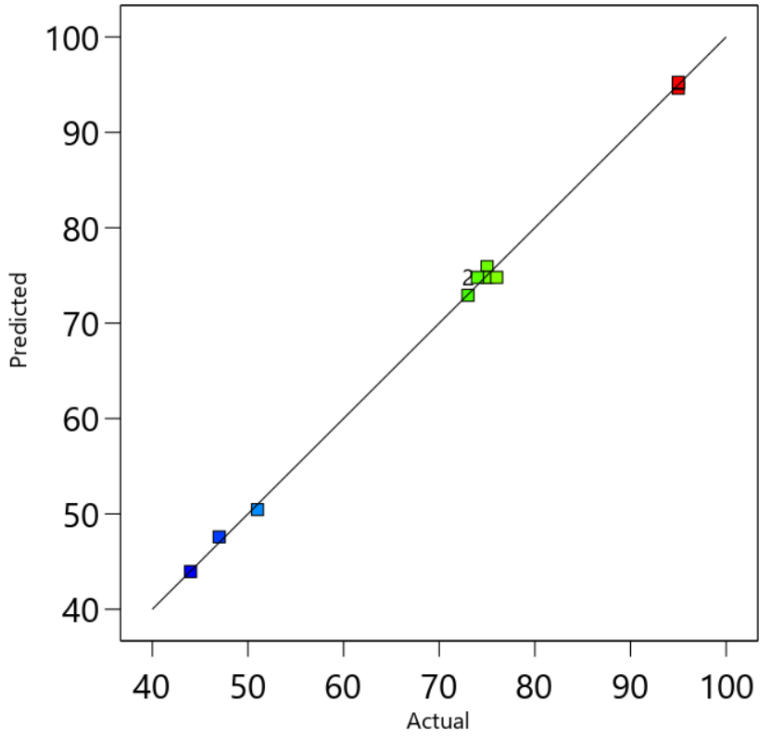

Fig. 4: Comparison of the developed model (predicted) with experimental data (Actual)

Fig. 5 illustrates the contour plot of magnesium precipitation as a function of NaOH concentration and temperature. The results indicate that the effect of temperature is significantly lower than that of NaOH concentration. This is because the variation in NaOH concentration has a stronger influence on magnesium precipitation, showing that the process is mainly dependent on NaOH concentration.

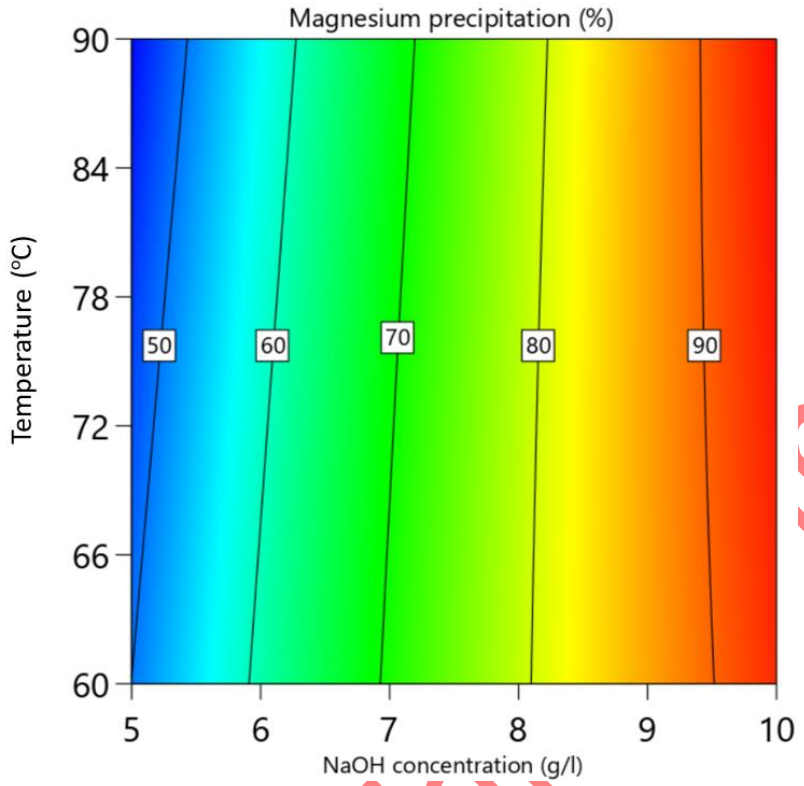

Fig. 5: Interaction effect of NaOH concentration and temperature on magnesium precipitation

3.2. Process simulation results

3.2.1. Physical properties

Investigation of physical properties is crucial for analyzing mass and energy balances. The properties of brine water can differ significantly from those of pure water and even seawater due to the presence of various dissolved minerals and compounds. Additionally, the concentration of these components increases in the recovery section as pure water is removed, resulting in more concentrated brine. Fig. 6a to Fig. 6f illustrate the variation of density, specific heat capacity, surface tension, thermal conductivity, viscosity, and pH of brine water as a function of temperature. As shown in Fig. 6a, the density of brine water decreases with increasing temperature and approaches that of pure water. This indicates that the behavior of brine density becomes more similar to pure water at higher temperatures. Fig. 6b shows that the specific heat capacity of brine water is generally lower than that of pure water. Although the variation is not large, a nonlinear trend is observed due to the complex temperature dependence of heat capacity. According to Fig. 6c and Fig. 6d, the surface tension and thermal conductivity of brine water behave similarly to pure water. The presence of minerals has no significant effect on these two properties within the tested temperature range. As illustrated in Fig. 6e, the viscosity of brine water is slightly higher than that of pure water, but the overall trend with temperature remains similar. Finally, Fig. 6f shows that the pH of brine water

decreases as temperature increases. This is an important result, as pH plays a critical role in mineral precipitation during alkaline treatment.

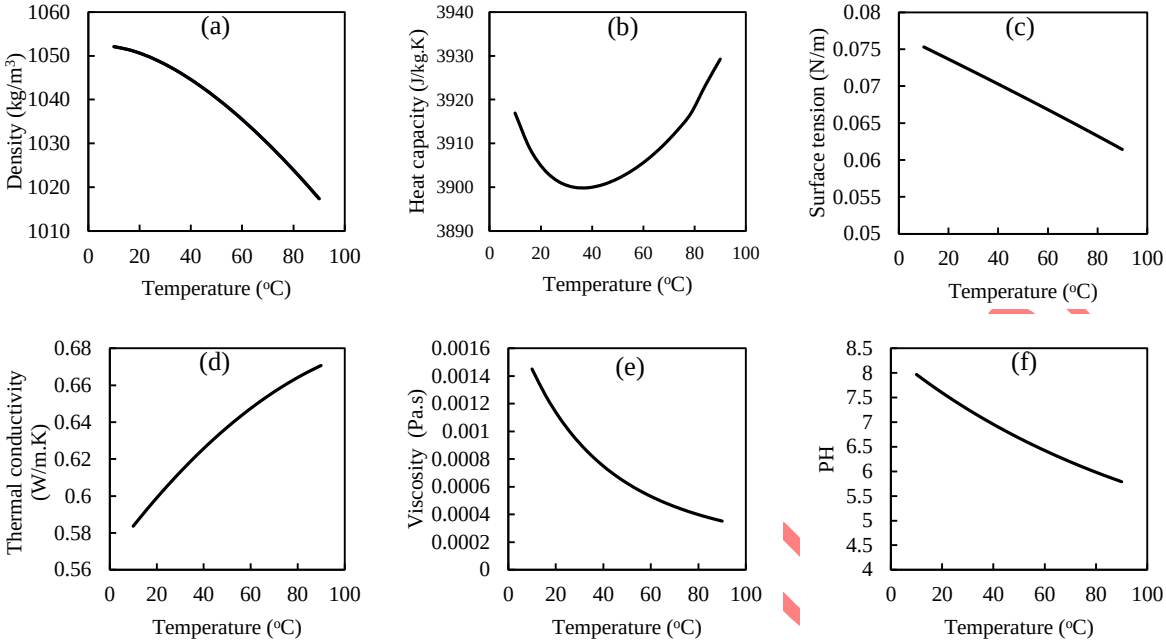

Fig. 6: Variation of brine water physical properties with temperature: (a) density, (b) specific heat capacity, (c) surface tension, (d) thermal conductivity, (e) viscosity, and (f) pH.

Fig. ٧ presents the variation in specific heat capacity for MgO and $Mg(OH)_2$ within the temperature range of ١٠٠ to ٤٠٠ °C. The results indicate that the heat capacity increases for both solids as temperature rises, which is consistent with typical thermal behavior of solid materials. Notably, $Mg(OH)_2$ shows a higher heat capacity than MgO throughout the entire range, with values approximately 50 percent greater. This difference is important in process design, particularly in thermal energy calculations.

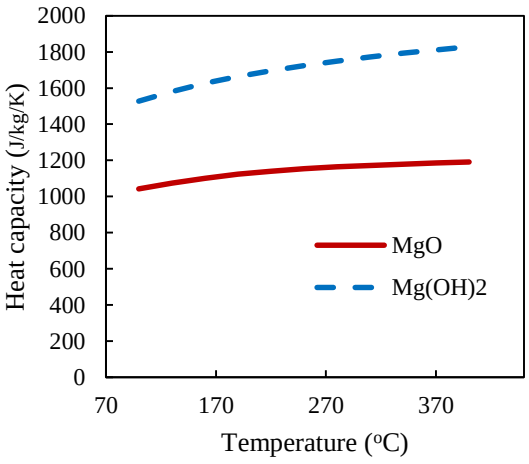

Fig. ٧: Specific heat capacity of MgO and $Mg(OH)_2$ as a function of temperature

3.2.2. Effect of feed flow rate

In this section, the effect of varying feed flow rates at a constant temperature of 60°C and NaOH concentration of ٧٫٥ g/L is examined on four key parameters: NaOH consumption for $Mg^{+٢}$ precipitation, $Mg(OH)_2$ production, MgO production, and the net energy consumption of the entire process.

As shown in Fig. 8a, increasing the feed flow rate leads to higher NaOH consumption. This occurs because a higher flow rate contains more dissolved $Mg^{+٢}$, requiring more NaOH to achieve full precipitation. For instance, when the feed flow rate increases from ٥٠,٠٠٠ m^3/day to ١٠٠,٠٠٠ m^3/day, the NaOH consumption rises from ٣٧٥ ton/day to ٧٥٠ ton/day.

Fig. ٨b and Fig. ٨c show that the production of $Mg(OH)_2$ and MgO also increases with feed flow rate. This is due to the greater availability of $Mg^{+٢}$ at higher volumes, which results in more precipitation and subsequent conversion. Specifically, $Mg(OH)_2$ production increases from ١٣١ ton/day at ٥٠,٠٠٠ m^3/day to ٢٦٣ tone/day at ١٠٠,٠٠٠ m^3/day, while MgO production increases from ٩١ ton/day to ١٨٢ ton/day.

Finally, Fig. 8d illustrates the trend in net energy consumption. As the feed flow rate increases, the energy requirement also rises due to the larger volume of brine entering the system at ٦٠°C. The net energy consumption increases from ١٢٠٠٠ kW at ٥٠,٠٠٠ m^3/day to ٤٤٠٠٠ kW at ١٠٠,٠٠٠ m^3/day.

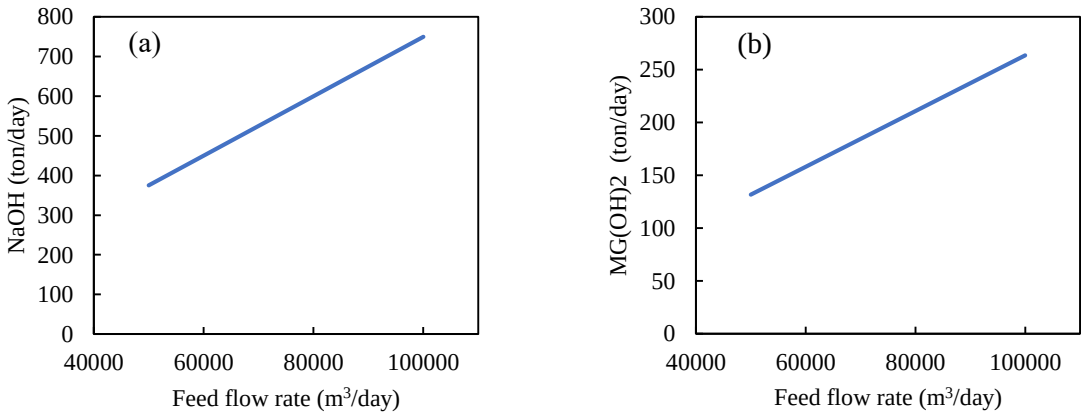

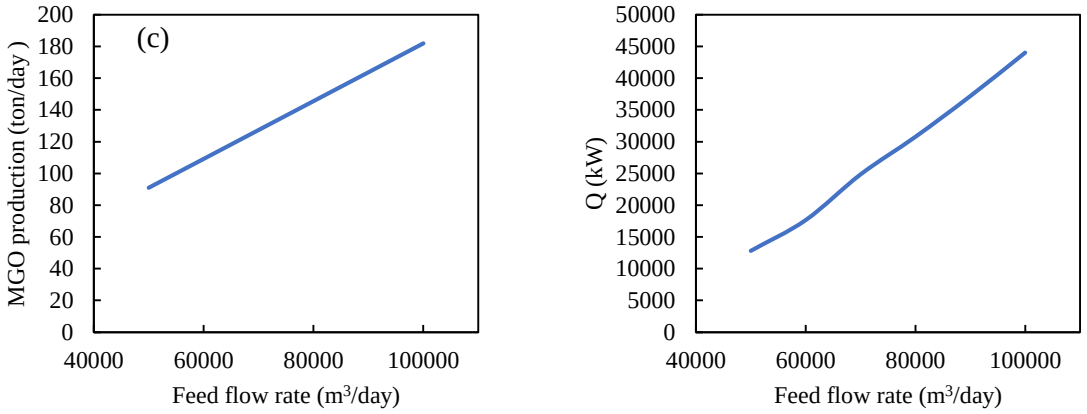

Fig. ٨: Effect of feed flow rate on (a) NaOH consumption, (b) $Mg(OH)_2$ production, (c) MgO production, and (d) net energy consumption at 60°C.

3.2.3. Effect of precipitation temperature

In this section, the effect of temperature on key factors is investigated. The NaOH concentration was considered ٧,٥ g/L, and the feed flow rate was set at ٧٥,٠٠٠ m^3/day. Since the feed flow rate and NaOH concentration are constant, the effect of temperature on NaOH consumption is not analyzed, as it remains almost unchanged. Instead, this section focuses on the production of $Mg(OH)_2$, MgO, and net energy consumption.

Fig. ٩a shows the effect of precipitation temperature on $Mg(OH)_2$ production. Between ٦٠ °C and ٩٠ °C, the production remains relatively stable. As the temperature increases from ٦٠ °C to ٧٥ °C, $Mg(OH)_2$ production increases slightly. However, when the temperature rises from ٧٥ °C to ٩٠ °C, the production decreases. Overall, the $Mg(OH)_2$ production remains almost constant at around ٢٠٩ ton/day. Fig. ٩b shows that MgO production first increases and then decreases with increasing precipitation temperature. Since MgO is obtained from the calcination of $Mg(OH)_2$, its production follows the same trend. Overall, MgO production remains almost constant at around 144 ton/day. Fig. 9c presents the effect of temperature on net energy consumption. As expected, the energy requirement rises sharply with increasing temperature due to the additional thermal energy needed to heat the brine feed. When the temperature increases from 60 °C to 90 °C, the net energy consumption increases by approximately 2.3 times.

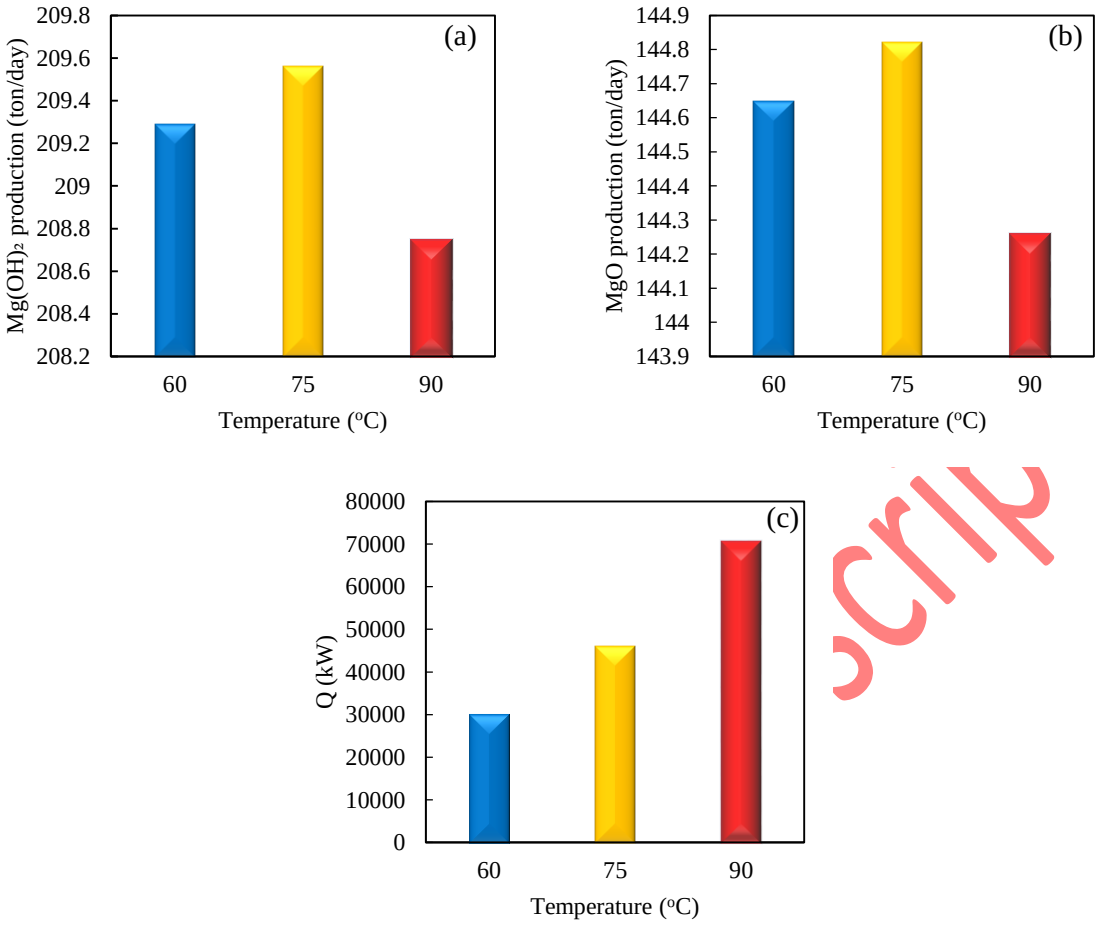

Fig. ٩: Effect of precipitation temperature on (a) Mg $(OH)_2$ production, (b) MgO production, and (c) net energy consumption at a constant feed flow rate of ٧٥٠٠٠,٠٠٠ *m³/day.*

3.2.4. Effect of NaOH concentration

Fig. 10a illustrates the effect of NaOH concentration on NaOH consumption at a feed flow rate of 75,000 L/h and a precipitation temperature of 75 °C. When the NaOH concentration increases from ٥ g/L to ١٠ g/L, NaOH consumption rises from ٣٧٥ ton/day to ٧٥٠ ton/day, representing a twofold increase. This shows that NaOH concentration and its consumption are directly related—higher concentrations lead to greater reagent utilization due to their interdependent nature in the precipitation process.

Fig. ١٠b shows the effect of NaOH concentration on $Mg(OH)_2$ production under the same operating conditions. As the NaOH concentration increases from ٥ g/L to ١٠ g/L, $Mg(OH)_2$ production increases from ١٢٦,٦ ton/day to ٢٥٥,٤ ton/day, also corresponding to a twofold rise. This occurs because higher NaOH concentration enhances the precipitation of magnesium ions, resulting in a higher yield of $Mg(OH)_2$.

Fig. ١٠c presents the variation of MgO production with NaOH concentration. Since MgO is obtained from the calcination of $Mg(OH)_2$, its production follows the same pattern. Increasing the NaOH concentration from 5 g/L to 10 g/L raises MgO output from 87.5 ton/day to 176.5

ton/day, reflecting the direct dependence of MgO yield on the extent of magnesium precipitation.

Fig. 10d depicts the effect of NaOH concentration on net energy consumption. The influence of NaOH concentration on energy demand is relatively small because the increase in solid production does not significantly affect the remaining brine flow. However, a slight decrease in total energy consumption is observed as the NaOH concentration increases. This reduction, approximately 3.7% when the concentration rises from 5 g/L to 10 g/L, is attributed to the higher condensate water flow that can be recovered and reused within the system, thereby enhancing overall energy efficiency.

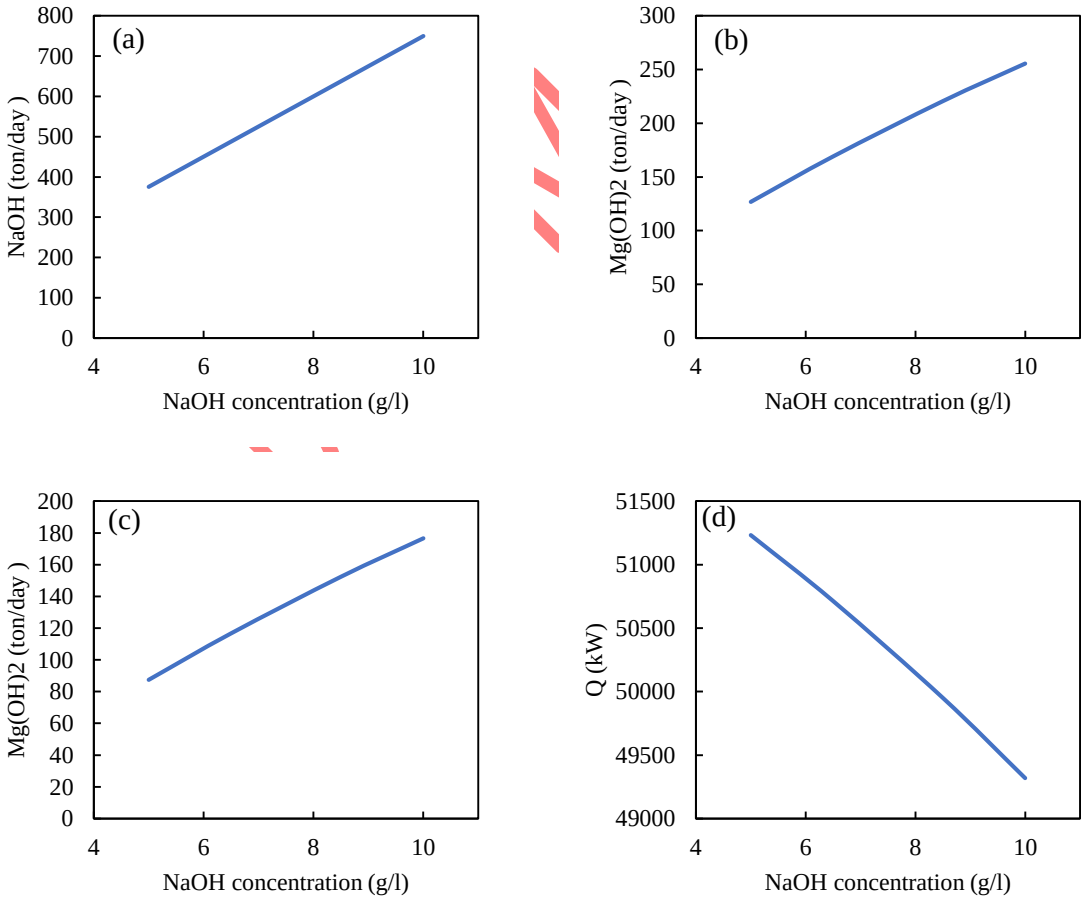

Fig. ١٠: Effect of NaOH concentration on (a) NaOH consumption, (b) $Mg(OH)_2$ production, (c) MgO production, and (d) net energy consumption at 75°C.

3.2.5. Pure water production

Figs. 11a, 11b, and 11c show the effects of feed flow rate, precipitation temperature, and NaOH concentration, respectively, on water production from the overall process. In Fig. ١١a, at a precipitation temperature of ٧٥ °C and NaOH concentration of ٧٫٥ g/L, increasing the feed flow rate leads to higher water production due to the larger solvent volume and greater mass of precipitated products such as $Mg(OH)_2$ and MgO. Specifically, when the flow rate increases from ٥٠,٠٠٠ m^3/day to ١٠٠,٠٠٠ m^3/day, water production doubles from ١٥٠ m^3/day to ٣٠٠ m^3/day.

Fig. 11b illustrates the effect of precipitation temperature at a feed flow rate of 75,000 m^3/day and an NaOH concentration of ٧٫٥ g/L. Increasing the precipitation temperature does not significantly change the $Mg(OH)_2$ yield. For example, raising the temperature from ٦٠ °C to 90 °C results in a water output of about 253 m^3/day.

Fig. ١١c depicts the influence of NaOH concentration at a feed flow rate of ٧٥,٠٠٠ m^3/day and precipitation temperature of ٧٥ °C. As the NaOH concentration increases from ٥ g/L to ١٠ g/L, water production also rises. This occurs because higher NaOH concentrations enhance $Mg(OH)_2$ precipitation, which in turn increases the formation of water vapor during calcination. Increasing the concentration from 5 g/L to 10 g/L doubles water production.

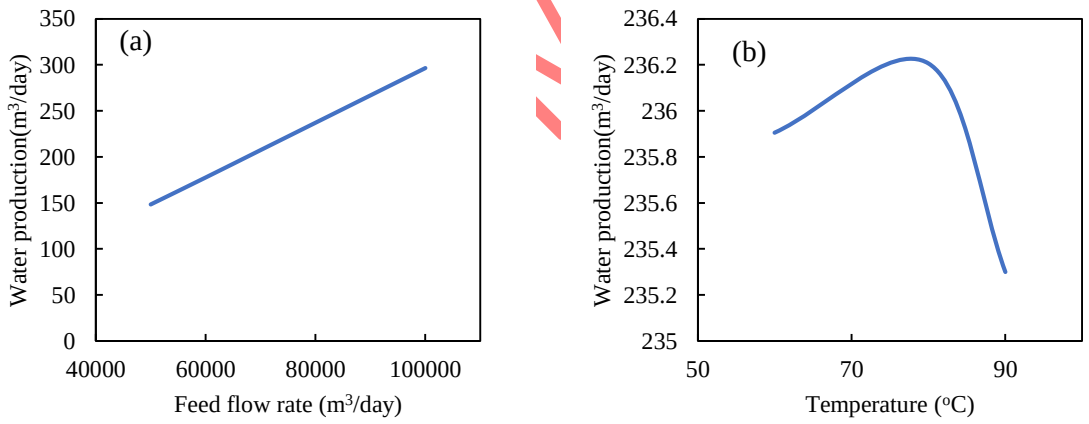

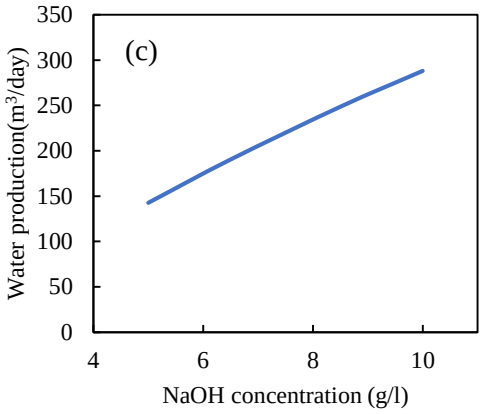

Fig. 11: Effect of (a) feed flow rate (b) precipitation temperature and (c) NaOH concentration on water production from the calcination reactor.

4. Economic Analysis

This section presents an economic analysis of the proposed process as a function of precipitation temperature and feed flow rate. The total process cost includes three main components: material cost, primarily the cost of NaOH used for Mg^{+2} precipitation; energy cost, mainly for heating the brine to the desired temperature; and operational and maintenance costs, assumed to be 5% of the total operation cost. The capital cost is significantly lower compared to the operational cost and is therefore not considered in this analysis. For the analysis, The energy cost for heating is 3.32×10^{-6} USD/kJ [36]. The cost of NaOH is taken as 327 USD/ton [37]. For the purpose of this analysis, the selling price of MgO is assumed to be 3,000 USD/ ton [14]. The objective function of our analysis is as follows [36]:

$$F = RP - \sum_{j} C_i \tag{5}$$

Where R is the production rate of MgO, P is the selling price, and C is the total cost of production, which includes the costs of NaOH, energy, and maintenance. The objective of the economic analysis is to maximize the net profit, defined as the difference between revenue (R × P) and total costs ($\sum_j C_i$).

Figs. 12a, 12b, and 12c illustrate the effect of brine flow rate, precipitation temperature, and NaOH concentration on NaOH cost, energy cost, maintenance cost, and revenue, respectively. For investigating the effect of brine flow rate, the precipitation temperature was fixed at 75 °C and NaOH concentration at 7.5 g/L. To examine the effect of temperature or NaOH concentration, the feed flow rate was fixed at 75,000 m³/day.

According to Fig. 12a, all costs (NaOH, energy, and maintenance) and revenue increase with increasing feed flow rate. Higher flow rates require more energy input and greater NaOH consumption. Additionally, a higher flow rate provides more Mg^{+2} ions for precipitation, resulting in increased revenue. Specifically, as the flow rate increases from 5,000 m³/day to

100,000 m³/day, NaOH cost nearly doubles, energy cost increases by 3.43 times, maintenance cost doubles, and revenue approximately doubles. These results highlight that the energy requirement is the most sensitive factor to changes in feed flow rate, emphasizing the importance of process integration strategies such as heat recovery from effluent streams to reduce overall energy demand.

Fig. 12b shows the effect of precipitation temperature. As the temperature increases, energy costs rise significantly, while other costs remain almost constant. The maintenance cost changes only slightly, and revenue decreases due to higher energy consumption. For example, increasing the temperature from 60 °C to 90 °C leaves the NaOH cost nearly unchanged, but the energy cost increases by about 2.8 times, resulting in a 5.6% decrease in revenue. These results indicate that precipitation temperature has a much stronger effect on energy consumption than on other cost factors. To better assess the overall impact, it is important to consider the objective function (net value), which is discussed in the optimization section. Fig. 12c presents the effect of NaOH concentration. Energy cost remains nearly constant as NaOH concentration increases, but maintenance cost, NaOH consumption, and revenue all rise. Higher NaOH concentration increases reagent consumption, requires additional maintenance, and enhances $Mg(OH)_2$ production, thereby increasing revenue. Specifically, as NaOH concentration increases from 5 g/L to 10 g/L, NaOH consumption cost doubles, maintenance cost rises by 89%, and revenue increases by 117%.

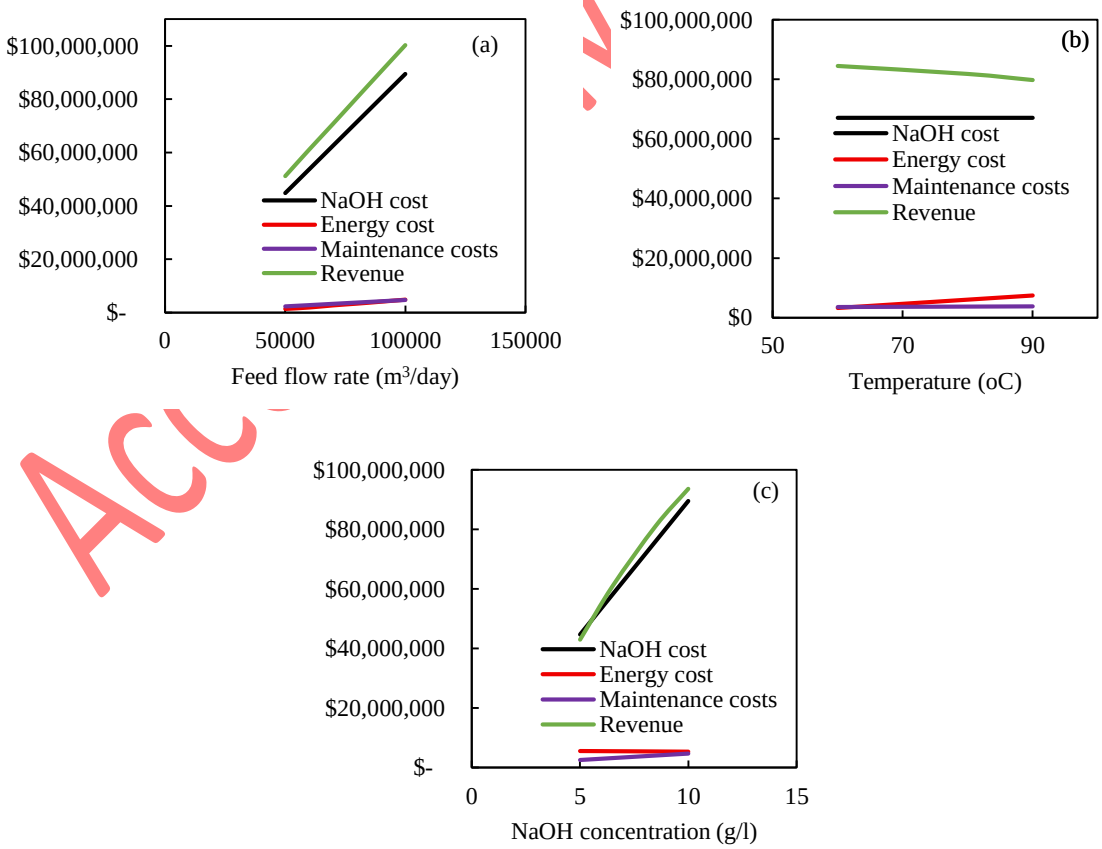

Fig. 12: Effect of (a) brine feed flow rate, (b) precipitation temperature, and (c) NaOH concentration on NaOH cost, energy cost, maintenance cost, and revenue.

5. Optimization

In this section, the objective function (Eq. 4) is optimized as a function of feed flow rate, NaOH concentration, and precipitation temperature. For this purpose, the RSM method is again used to develop a quadratic equation for the objective function as a function of the considered factors, and then it is optimized. Additionally, the repetition of the center point is set to one because the objective function is calculated from simulations, and each repetition produces the same result. The simulation results and their corresponding outcomes are presented in Table 5.

Table 5: Objective function run design and corresponding results

A: NaOH concentration (g/l)	B: Temperature (°C)	C: Feed flow rate (m^3/day)	Objective function
10	60	100000	$131,131,000
7.5	90	75000	$79,877,400
5	75	75000	$51,082,600
10	60	50000	$66,604,000
7.5	75	100000	$109,023,000
7.5	60	75000	$84,539,100
5	60	100000	$74,519,400
10	90	50000	$68,863,200
5	90	100000	$58,095,500
7.5	75	50000	$56,089,800
10	75	75000	$100,577,000
5	60	50000	$38,295,800
5	90	50000	$31,202,300
7.5	75	75000	$82,670,100

Table 6 illustrates the ANOVA analysis of the developed objective function. According to the p-values and F-values, all factors have a significant effect on the objective function, except for the quadratic terms B^2 and C^2, which are statistically insignificant.

Table 6: ANOVA analysis for the developed objective function

Source	F-value	p-value
Model	353.070	< 0.0001
A: NaOH (g/l)	1495.470	< 0.0001
B: Temperature (°C)	13.670	0.014
C: Feed flow rate (m^3/day)	1468.200	< 0.0001
AB	24.020	0.0045
AC	132.840	< 0.0001
BC	2.660	0.1641
A^2	29.370	0.0029
B^2	0.132	0.7315
C^2	0.008	0.9341

Equations 5 and 6 illustrate the objective function.

$$Pc=82666896 + 24737637 \times A - 2365500 \times B + 24511029 \times C + 3505217 \times A\,B + 8242919 \times A\,C - 1165588 \times B\,C - 6836123 \times A^2 - 457879 \times B^2 - 109659 \times C^2 \quad (6)$$

$$Pr=-17929922 + 9399814 \times A - 320373 \times B + 251 \times C + 93472 \times A\,B + 132 \times A\,C - 3.11 \times B\,C - 1093779 \times A^2 - 2035 \times B^2 - 0.000175 \times C^2 \quad (7)$$

In these equations, P_c is the objective function in coded form, and P_R is the objective function in real units. A, B, and C represent NaOH concentration, temperature, and feed flow rate. The factors are coded as −1 and 1 to see which has the most effect on the objective function. The coefficients show that NaOH concentration (A) and feed flow rate (B) have similar effects, while temperature has a smaller effect. The interaction between NaOH concentration and feed flow rate (BC) has a larger effect than the other interactions.

Fig. 13 illustrates the comparison between the predicted and simulated objective functions. The results show a very good agreement between the simulation and the predicted values, indicating that the developed model accurately represents the system behavior. This agreement is further confirmed by the R-squared value of 0.999, which is very close to 1, demonstrating the high reliability and predictive capability of the model.

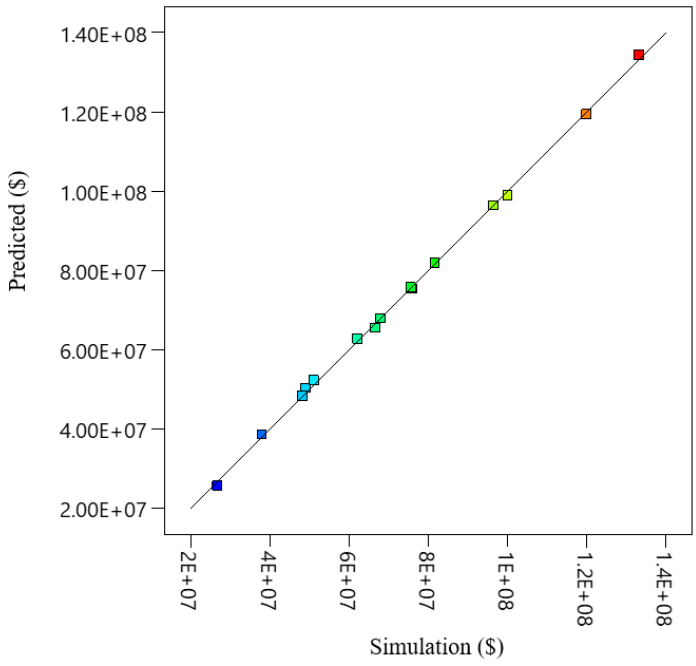

Fig. 13: Comparison of predicted and simulated objective function

Fig. 14 illustrates the interaction effect of feed flow rate and temperature on the objective function. It is evident that the effect of temperature is negative, while the effect of feed flow rate is positive. However, the influence of feed flow rate on the objective function is significantly higher than that of temperature. Additionally, the effect of feed flow rate shows a nonlinear behavior.

Fig. 15 shows the interaction effect of feed flow rate and NaOH concentration on the objective function. Both NaOH concentration and feed flow rate have a positive effect. The objective function increases significantly and nonlinearly as both the feed flow rate and NaOH concentration increase.

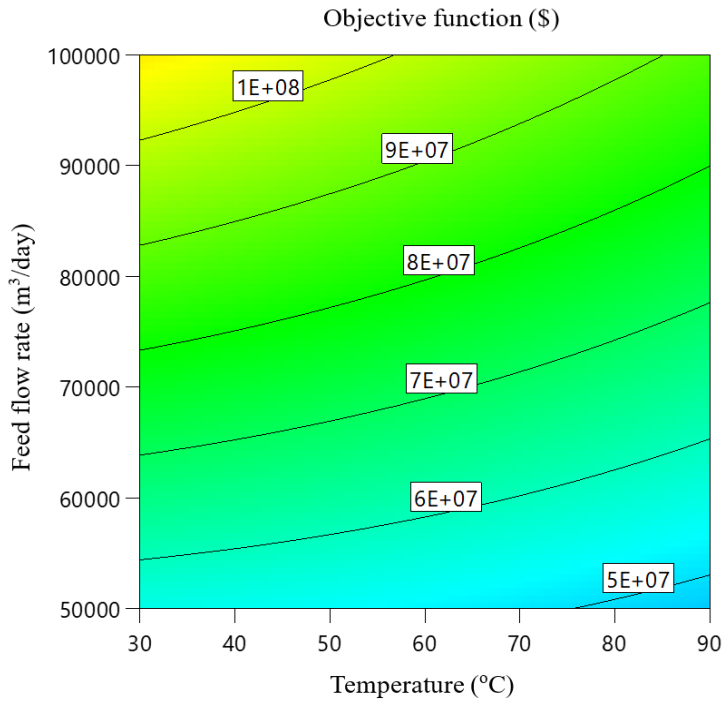

Fig. 14: Interaction effect of feed flow rate and temperature on the objective function

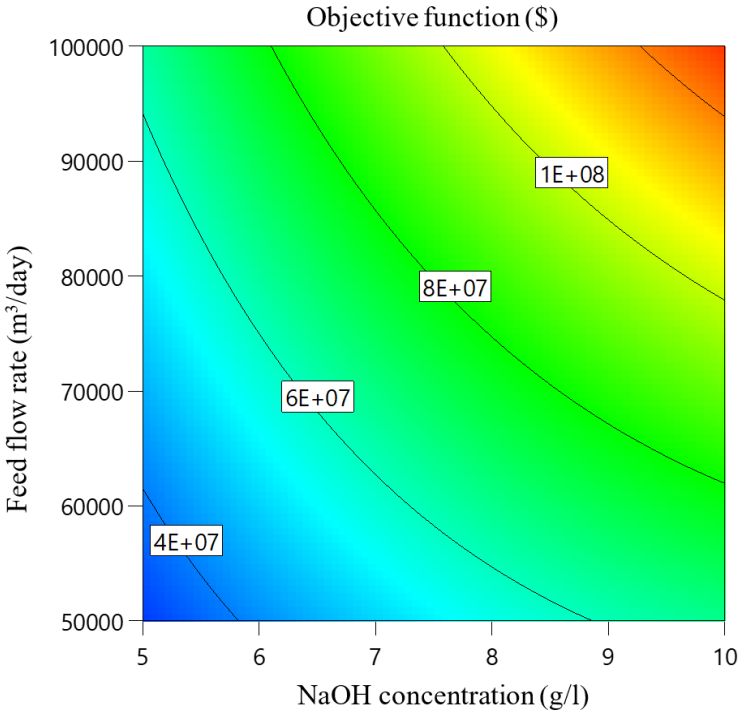

Fig. 15: Interaction effect of NaOH concentration and feed flow rate on the objective function

Table 7 shows the optimized value of the objective function along with the corresponding optimal values of NaOH concentration, temperature, and feed flow rate. It is evident that the objective function is maximized when the NaOH concentration and feed flow rate are at their highest values, while the temperature is at its minimum.

Table 7: Optimized value of the objective function

Factor	A (g/l)	B (°C)	C (m^3/day)	Objective function
Value	10	60	100000	$133,213,000.

6. Conclusions

This study investigates magnesium recovery from seawater reverse osmosis (SWRO) brine through precipitation of Mg^{2+} as $Mg(OH)_2$ followed by calcination to MgO, combining experimental work with Aspen Plus process simulation and economic analysis. The experimental results show that NaOH concentration is the dominant factor affecting magnesium precipitation, while temperature has a comparatively weaker influence. Increasing NaOH concentration significantly enhances Mg^{2+} removal and leads to higher production of both $Mg(OH)_2$ and MgO. The thermophysical behavior of brine is generally similar to that of pure water, except for a slightly lower specific heat capacity, indicating that the heating demand is only marginally reduced compared to pure water. Process simulation results indicate that increasing feed flow rate enhances $Mg(OH)_2$ and MgO production but simultaneously increases NaOH consumption and energy demand due to the larger processing volume. Higher precipitation temperatures slightly reduce magnesium recovery and substantially increase

energy consumption, whereas increasing NaOH concentration improves overall recovery and slightly reduces net energy demand due to enhanced heat recovery from water vapor during calcination. Water generation during calcination also increases with higher feed flow rates and NaOH concentrations, contributing additional value to the process. From an economic perspective, the highest net profit is achieved at a feed flow rate of 100,000 m^3/day, low precipitation temperature (60 °C), and high NaOH concentration, resulting in an estimated annual profit of approximately 133 million USD. Overall, feed flow rate and NaOH concentration have a stronger influence on process profitability than temperature, indicating that maximizing these parameters is most beneficial for system performance. The results confirm the technical and economic feasibility of large-scale MgO production from RO brine and support its potential for industrial brine valorization. Future work should focus on improving process sustainability through energy integration strategies such as waste heat recovery, process intensification, and advanced brine management techniques to further reduce operational costs and environmental impact.

Nomenclature

Symbol	Description	Unit	Symbol	Description	Unit
A	NaOH concentration	g/L	**Mg^{2+}**	Magnesium ion in aqueous solution	mg/L
B	Precipitation temperature	°C	**$Mg(OH)_2$**	Magnesium hydroxide	–
C	Feed flow rate	m^3/day	**MgO**	Magnesium oxide	–
OH^-	Hydroxide ion	–	**TDS**	Total dissolved solids	ppm
F	Objective function (net profit)	USD	**P**	Selling price of MgO	USD/ton
ANOVA	Analysis of variance	–	**RSM**	Response Surface Methodology	–
CCD	Central Composite Design	–	**F-value**	Fisher statistical value	–
p-value	Statistical significance level	–	**R^2**	Coefficient of determination	–

References

[1] M. Abrofarakh, H. Moghadam, H.K. Abdulrahim, Investigation of direct contact membrane distillation (DCMD) performance using CFD and machine learning approaches, Chemosphere, 357 (2024) 141969. https://doi.org/10.1016/j.chemosphere.2024.141969.

[2] M. Salman, M. Ahmed, H. Al-Sairfi, Y. Al-Foudari, Mineral Extraction from Mixed Brine Solutions, Separations, 12 (2025) 266. https://doi.org/10.3390/separations12100266.

[3] D.B. Agusdinata, W. Liu, H. Eakin, H. Romero, Socio-environmental impacts of lithium mineral extraction: towards a research agenda, Environmental Research Letters, 13 (2018) 123001. https://doi.org/10.1088/1748-9326/aae4df.

[4] M. Abrofarakh, Effect of incorporating Sulzer SMV static mixers on the performance of direct contact membrane distillation (DCMD): A three-dimensional computational fluid dynamics (CFD) study, Separation and Purification Technology, 359 (2025) 130606. https://doi.org/10.1016/j.seppur.2024.130606.

[5] T. Jeppesen, L. Shu, G. Keir, V. Jegatheesan, Metal recovery from reverse osmosis concentrate, Journal of Cleaner Production, 17 (2009) 703-707. https://doi.org/10.1016/j.jclepro.2008.11.013.

[6] A. Mohammad, M. El-Naas, A. Al-Marzouqi, M. Suleiman, M. Al Musharfy, Optimization of magnesium recovery from reject brine for reuse in desalination post-treatment, Journal of Water Process Engineering, 31 (2019) 100810. https://doi.org/10.1016/j.jwpe.2019.100810.

[7] H. Dong, C. Unluer, E.-H. Yang, A. Al-Tabbaa, Recovery of reactive MgO from reject brine via the addition of NaOH, Desalination, 429 (2018) 88-95. https://doi.org/10.1016/j.desal.2017.12.021.

[8] L. Kumari, W. Li, C.H. Vannoy, R.M. Leblanc, D. Wang, Synthesis, characterization and optical properties of Mg(OH)2 micro-/nanostructure and its conversion to MgO, Ceramics International, 35 (2009) 3355-3364. https://doi.org/10.1016/j.ceramint.2009.05.035.

[9] M. Chinthala, A. Balakrishnan, P. Venkataraman, V. Manaswini Gowtham, R.K. Polagani, Synthesis and applications of nano-MgO and composites for medicine, energy, and environmental remediation: a review, Environmental Chemistry Letters, 19 (2021) 4415-4454. https://doi.org/10.1007/s10311-021-01241-0.

[10] R.M. DuChanois, N.J. Cooper, B. Lee, S.K. Patel, L. Mazurowski, T.E. Graedel, M. Elimelech, Prospects of metal recovery from wastewater and brine, Nature Water, 1 (2023) 37-46. https://doi.org/10.1038/s44221-023-00006-7.

[11] O. Lehmann, O. Nir, M. Kuflik, O. Lahav, Recovery of high-purity magnesium solutions from RO brines by adsorption of Mg(OH)2 (s) on Fe3O4 micro-particles and magnetic solids separation, Chemical Engineering Journal, 235 (2014) 37-45. https://doi.org/10.1016/j.cej.2013.08.046.

[12] M.H. Sorour, H.A. Hani, H.F. Shaalan, G.A. Al-Bazedi, Schemes for salt recovery from seawater and RO brines using chemical precipitation, Desalination and Water Treatment, 55 (2015) 2398-2407. https://doi.org/10.1080/19443994.2014.923067

[13] S. Casas, C. Aladjem, E. Larrotcha, O. Gibert, C. Valderrama, J.L. Cortina, Valorisation of Ca and Mg by-products from mining and seawater desalination brines for water treatment applications, Journal of Chemical Technology & Biotechnology, 89 (2014) 872-883. https://doi.org/10.1002/jctb.4279.

[14] M. Ahmad, B. Garudachari, Y. Al-Wazzan, R. Kumar, J.P. Thomas, Mineral extraction from seawater reverse osmosis brine of Gulf seawater, Desalination and Water Treatment, 144 (2019) 45-56. https://doi.org/10.5004/dwt.2019.23679.

[15] M. Turek, W. Gnot, Precipitation of magnesium hydroxide from brine, Industrial & Engineering Chemistry Research, 34 (1995) 244-250. https://doi.org/10.1021/ie00040a025.

[16] N. Melián-Martel, J. Sadhwani, S.O.P. Báez, Saline waste disposal reuse for desalination plants for the chlor-alkali industry: The particular case of pozo izquierdo SWRO desalination plant, Desalination, 281 (2011) 35-41. https://doi.org/10.1016/j.desal.2011.07.040.

[17] N. Mahmud, D.V.F. Alvarez, M.H. Ibrahim, M.H. El-Naas, D.V. Esposito, Magnesium recovery from desalination reject brine as pretreatment for membraneless electrolysis, Desalination, 525 (2022) 115489. https://doi.org/10.1016/j.desal.2022.115489.

[18] F. Vassallo, D. La Corte, N. Cancilla, A. Tamburini, M. Bevacqua, A. Cipollina, G. Micale, A pilot-plant for the selective recovery of magnesium and calcium from waste brines, Desalination, 517 (2021) 115231. https://doi.org/10.1016/j.desal.2021.115231.

[19] A. Pérez-González, R. Ibáñez, P. Gómez, A. Urtiaga, I. Ortiz, J. Irabien, Recovery of desalination brines: separation of calcium, magnesium and sulfate as a pre-treatment step, Desalination and Water Treatment, 56 (2015) 3617-3625. https://doi.org/10.1080/19443994.2014.959076.

[20] B.S. Lalia, A. Khalil, R. Hashaikeh, Selective electrochemical separation and recovery of calcium and magnesium from brine, Separation and Purification Technology, 264 (2021) 118416. https://doi.org/10.1016/j.seppur.2021.118416.

[21] M.A. Ashraf, M. Usman, I. Hussain, F. Ahmad, S. Guo, L. Zhang, Lithium extraction from high magnesium salt lake brine with an integrated membrane technology, Separation and Purification Technology, 302 (2022) 122163. https://doi.org/10.1016/j.seppur.2022.122163.

[22] H. Dong, C. Unluer, E.-H. Yang, A. Al-Tabbaa, Synthesis of reactive MgO from reject brine via the addition of NH4OH, Hydrometallurgy, 169 (2017) 165-172. https://doi.org/10.1016/j.hydromet.2017.01.010.

[٢٣] C.A. Quist-Jensen, F. Macedonio, E. Drioli, Membrane crystallization for salts recovery from brine—an experimental and theoretical analysis, Desalination and Water Treatment, ٥٧ (٢٠١٦) ٧٥٩٣-7603. https://doi.org/10.1080/19443994.2015.1093521.

[24] S. Ruan, E.-H. Yang, C. Unluer, Production of reactive magnesia from desalination reject brine and its use as a binder, Journal of CO2 Utilization, 44 (2021) 101383. https://doi.org/10.1016/j.jcou.2020.101383.

[25] H.L. Senevirathna, W.C. Lee, S. Wu, K. Bai, P. Wu, Transforming desalination brine into highly reactive magnesium oxide and life cycle analysis, Watershed Ecology and the Environment, 7 (2025) 36-46. https://doi.org/10.1016/j.wsee.2025.01.001.

[26] F.Z. Karmil, A. Abbassi, O. Mounkachi, H. El Alaoui-Belghiti, S. Mountadar, A. Rich, M. Mountadar, Recovery of high reactive alkaline-earth-oxide (CaO and MgO) from reverse osmosis reject desalination brine: kinetics, equilibrium, cost-effectiveness and energy consumption, Waste Management Bulletin, 100218 (2025). https://doi.org/10.1016/j.wmb.2025.100218.

[٢٧] A. Saud, A. Ali, C.A. Quist-Jensen, Membrane distillation crystallization's parametric analysis for magnesium sulphate crystallization from simulated nanofiltration brine, Separation and Purification Technology, 133852 (2025). https://doi.org/10.1016/j.seppur.2025.133852.

[28] L. Ventimiglia, F. Vassallo, G.L. Burgio, A. Campione, L. Cammilli, P. Vicario, G. Battaglia, F. Vicari, A. Cipollina, A. Tamburini, Pilot scale production of Mg(OH)2 compounds from a real industrial reverse osmosis desalination brine, Desalination, 119052 (2025). https://doi.org/10.1016/j.desal.2025.119052.

[29] F.Z. Karmil, S. Mountadar, H. El Alaoui-Belghiti, M.E. Belghiti, A. Zeroual, A. Rich, M. Mountadar, Synthesis of magnesia-modified magnetite from desalination reject brine for enhanced phosphate removal in aqueous solution: experimental studies supported by DFT/MD simulations,

safety, and cost analysis, Inorganic Chemistry Communications, 177 (2025) 114364. https://doi.org/10.1016/j.inoche.2025.114364.

[30] P. Lu, P. Ochonma, M. Kim, C. Walike, A. Sunkara, G. Gadikota, Electrochemical recovery of high-purity calcium carbonate and magnesium hydroxide from brine via carbon mineralization, MRS Bulletin, 50 (2025) 20-31. https://doi.org/10.1557/s43577-024-00804-8.

[31] X. Xiao, H.S. Santoso, C. Unluer, E.-H. Yang, The use of waste concrete sludge as alkali source to recover reactive MgO from reject brine, Desalination, 600 (2025) 118470. https://doi.org/10.1016/j.desal.2024.118470.

[32] T. Kopac, Y. Demirel, Optimizing CO2 capture from biogas: a comparative study of amine-based solvents through Aspen Plus simulations, Biomass Conversion and Biorefinery (2025) 1-21. https://doi.org/10.1007/s13399-025-06668-5.

[33] T. Nakagaki, H. Isogai, H. Sato, J. Arakawa, Updated e-NRTL model for high-concentration MEA aqueous solution by regressing thermodynamic experimental data at high temperatures, International Journal of Greenhouse Gas Control, 82 (2019) 117-126. https://doi.org/10.1016/j.ijggc.2019.02.007.

[34] A. Deshmukh, A.D. Wilson, J.H. Lienhard, Electrically powered high-salinity brine separation using dimethyl ether, Industrial & Engineering Chemistry Research, 63 (2024) 8341-8356. https://doi.org/10.1021/acs.iecr.4c01654.

[35] Z. Pan, C. Zhao, Dehydration/hydration of MgO/H2O chemical thermal storage system, Energy, 82 (2015) 611-618. https://doi.org/10.1016/j.energy.2015.01.026.

[36] Z. Du, E.-H. Yang, C. Unluer, Investigation of the properties of Mg(OH)2 extracted from magnesium-rich brine via the use of an industrial by-product, Cement and Concrete Composites, 152 (2024) 105658. https://doi.org/10.1016/j.cemconcomp.2024.105658.

[37] M. Alsaffar, M. Ardakani, Y.M. Al-Abdullah, Analyzing decarbonization policies targeting interdependent electric power and water desalination infrastructure: A case study for Kuwait, Energy for Sustainable Development, 86 (2025) 101715. https://doi.org/10.1016/j.esd.2025.101715.

[38] R.R. Contreras, J. Almarza, L. Rincon, C. Ruiz, Green sodium hydroxide for industrial purposes. A short review, Journal of Environmental Chemical Engineering, 13 (2025) 114972. https://doi.org/10.1016/j.jece.2024.114972.

[1] M. Abrofarakh, H. Moghadam, H.K. Abdulrahim, Investigation of direct contact membrane distillation (DCMD) performance using CFD and machine learning approaches, Chemosphere, 357 (2024) 141969.
[2] M. Salman, M. Ahmed, H. Al-Sairfi, Y. Al-Foudari, Mineral Extraction from Mixed Brine Solutions, Separations, 12 (2025) 266.
[3] D.B. Agusdinata, W. Liu, H. Eakin, H. Romero, Socio-environmental impacts of lithium mineral extraction: towards a research agenda, Environmental Research Letters, 13 (2018) 123001.
[4] M. Abrofarakh, Effect of incorporating Sulzer SMV static mixers on the performance of direct contact membrane distillation (DCMD): A three-dimensional computational fluid dynamics (CFD) study, Separation and Purification Technology, 359 (2025) 130606.
[5] T. Jeppesen, L. Shu, G. Keir, V. Jegatheesan, Metal recovery from reverse osmosis concentrate, Journal of Cleaner Production, 17 (2009) 703-707.

[6] A. Mohammad, M. El-Naas, A. Al-Marzouqi, M. Suleiman, M. Al Musharfy, Optimization of magnesium recovery from reject brine for reuse in desalination post-treatment, Journal of Water Process Engineering, 31 (2019) 100810.
[7] H. Dong, C. Unluer, E.-H. Yang, A. Al-Tabbaa, Recovery of reactive MgO from reject brine via the addition of NaOH, Desalination, 429 (2018) 88-95.
[8] L. Kumari, W. Li, C.H. Vannoy, R.M. Leblanc, D. Wang, Synthesis, characterization and optical properties of Mg (OH) 2 micro-/nanostructure and its conversion to MgO, Ceramics International, 35 (2009) 3355-3364.
[9] M. Chinthala, A. Balakrishnan, P. Venkataraman, V. Manaswini Gowtham, R.K. Polagani, Synthesis and applications of nano-MgO and composites for medicine, energy, and environmental remediation: a review, Environmental Chemistry Letters, 19 (2021) 4415-4454.
[10] R.M. DuChanois, N.J. Cooper, B. Lee, S.K. Patel, L. Mazurowski, T.E. Graedel, M. Elimelech, Prospects of metal recovery from wastewater and brine, Nature Water, 1 (2023) 37-46.
[11] O. Lehmann, O. Nir, M. Kuflik, O. Lahav, Recovery of high-purity magnesium solutions from RO brines by adsorption of Mg (OH) 2 (s) on Fe3O4 micro-particles and magnetic solids separation, Chemical Engineering Journal, 235 (2014) 37-45.
[12] M.H. Sorour, H.A. Hani, H.F. Shaalan, G.A. Al-Bazedi, Schemes for salt recovery from seawater and RO brines using chemical precipitation, Desalination and Water Treatment, 55 (2015) 2398-2407.
[١٣] S. Casas, C. Aladjem, E. Larrotcha, O. Gibert, C. Valderrama, J.L. Cortina, Valorisation of Ca and Mg by-products from mining and seawater desalination brines for water treatment applications, Journal of Chemical Technology & Biotechnology, 89 (2014) 872-883.
[14] M. Ahmad, B. Garudachari, Y. Al-Wazzan, R. Kumar, J.P. Thomas, Mineral extraction from seawater reverse osmosis brine of Gulf seawater, Desalination and Water Treatment, 144 (2019) 45-56.
[15] M. Turek, W. Gnot, Precipitation of magnesium hydroxide from brine, Industrial & engineering chemistry research, 34 (1995) 244-250.
[16] N. Melián-Martel, J. Sadhwani, S.O.P. Báez, Saline waste disposal reuse for desalination plants for the chlor-alkali industry: The particular case of pozo izquierdo SWRO desalination plant, Desalination, 281 (2011) 35-41.
[17] M.A. Ashraf, M. Usman, I. Hussain, F. Ahmad, S. Guo, L. Zhang, Lithium extraction from high magnesium salt lake brine with an integrated membrane technology, Separation and Purification Technology, 302 (2022) 122163.
[18] H. Dong, C. Unluer, E.-H. Yang, A. Al-Tabbaa, Synthesis of reactive MgO from reject brine via the addition of NH4OH, Hydrometallurgy, 169 (2017) 165-172.
[19] X. Xiao, H.S. Santoso, C. Unluer, E.-H. Yang, The use of waste concrete sludge as alkali source to recover reactive MgO from reject brine, Desalination, 600 (2025) 118470.
[20] N. Mahmud, D.V.F. Alvarez, M.H. Ibrahim, M.H. El-Naas, D.V. Esposito, Magnesium recovery from desalination reject brine as pretreatment for membraneless electrolysis, Desalination, 525 (2022) 115489.
[21] F. Vassallo, D. La Corte, N. Cancilla, A. Tamburini, M. Bevacqua, A. Cipollina, G. Micale, A pilot-plant for the selective recovery of magnesium and calcium from waste brines, Desalination, 517 (2021) 115231.
[22] A. Pérez-González, R. Ibáñez, P. Gómez, A. Urtiaga, I. Ortiz, J. Irabien, Recovery of desalination brines: separation of calcium, magnesium and sulfate as a pre-treatment step, Desalination and Water Treatment, 56 (2015) 3617-3625.
[23] B.S. Lalia, A. Khalil, R. Hashaikeh, Selective electrochemical separation and recovery of calcium and magnesium from brine, Separation and Purification Technology, 264 (2021) 118416.
[٢٤] C.A. Quist-Jensen, F. Macedonio, E. Drioli, Membrane crystallization for salts recovery from brine—an experimental and theoretical analysis, Desalination and Water Treatment, 57 (2016) 7593-7603.
[25] F.Z. Karmil, A. Abbassi, O. Mounkachi, H. El Alaoui-Belghiti, S. Mountadar, A. Rich, M. Mountadar, Recovery of high reactive alkaline-earth-oxide (CaO and MgO) from reverse osmosis reject desalination

brine: Kinetics, equilibrium, cost-effectiveness and energy-consumption, Waste Management Bulletin, DOI (2025) 100218.
[٢٦] A. Saud, A. Ali, C.A. Quist-Jensen, Membrane distillation crystallization's parametric analysis for magnesium sulphate crystallization from simulated nanofiltration brine, Separation and Purification Technology, DOI (2025) 133852.
[27] L. Ventimiglia, F. Vassallo, G.L. Burgio, A. Campione, L. Cammilli, P. Vicario, G. Battaglia, F. Vicari, A. Cipollina, A. Tamburini, Pilot scale production of Mg (OH) 2 compounds from a real industrial reverse osmosis desalination brine, Desalination, DOI (2025) 119052.
[28] F.Z. Karmil, S. Mountadar, H. El Alaoui-Belghiti, M.E. Belghiti, A. Zeroual, A. Rich, M. Mountadar, Synthesis of magnesia-modified magnetite from desalination reject brine for enhanced phosphate removal in aqueous solution: Experimental studies supported by DFT/MD simulations, safety, and cost analysis, Inorganic Chemistry Communications, 177 (2025) 114364.
[29] P. Lu, P. Ochonma, M. Kim, C. Walike, A. Sunkara, G. Gadikota, Electrochemical recovery of high-purity calcium carbonate and magnesium hydroxide from brine via carbon mineralization, MRS Bulletin, 50 (2025) 20-31.
[30] A. Smahi, M. Kanniche, N. Jourdan, C. Bouallou, O. Authier, CO2 Capture in MDEA-PZ and AMP-PZ Solvents: ELECNRTL vs. ENRTL-RK Models and Their Efficiency in Natural Gas Combined Cycles, ENRTL-RK Models and Their Efficiency in Natural Gas Combined Cycles (November 19, 2024), DOI (2024).
[31] T. Kopac, Y. Demirel, Optimizing CO2 capture from biogas: a comparative study of amine-based solvents through Aspen Plus simulations, Biomass Conversion and Biorefinery, DOI (2025) 1-21.
[32] T. Nakagaki, H. Isogai, H. Sato, J. Arakawa, Updated e-NRTL model for high-concentration MEA aqueous solution by regressing thermodynamic experimental data at high temperatures, International Journal of Greenhouse Gas Control, 82 (2019) 117-126.
[33] A. Deshmukh, A.D. Wilson, J.H. Lienhard, Electrically powered high-salinity brine separation using dimethyl ether, Industrial & Engineering Chemistry Research, 63 (2024) 8341-8356.
[34] Z. Pan, C. Zhao, Dehydration/hydration of MgO/H2O chemical thermal storage system, Energy, 82 (2015) 611-618.
[35] Z. Du, E.-H. Yang, C. Unluer, Investigation of the properties of Mg (OH) 2 extracted from magnesium-rich brine via the use of an industrial by-product, Cement and Concrete Composites, 152 (2024) 105658.
[36] M. Alsaffar, M. Ardakani, Y.M. Al-Abdullah, Analyzing decarbonization policies targeting interdependent electric power and water desalination infrastructure: A case study for Kuwait, Energy for Sustainable Development, 86 (2025) 101715.
[37] R.R. Contreras, J. Almarza, L. Rincon, C. Ruiz, Green sodium hydroxide for industrial purposes. A short review, Journal of Environmental Chemical Engineering, 13 (2025) 114972.